Raman and infrared reflectivity spectra of potassium lithium niobate single crystals

H. R. Xia, H. Yu,* and H. Yang†
Department of Physics, Shandong University, Jinan 250100, People's Republic of China

K. X. Wang and B. Y. Zhao
Institute of Physical Chemistry, Peking University, Beijing 100871, People's Republic of China

J. Q. Wei, J. Y. Wang, and Y. G. Liu
Institute of Crystal Materials, Shandong University, Jinan 250100, People's Republic of China
(Received 23 August 1996; revised manuscript received 17 January 1997)

The tetragonal tungsten bronze (TB) type potassium lithium niobate (KLN) single crystals were grown using the conventional pulling method. The molecular formula can be written as $K_{2.96}Li_{1.97}Nb_{5.07}O_{15}$ based on the crystal atomic absorption spectra. The lattice constants are $a=1.2575\pm0.0001$ nm and $c=0.3997\pm0.0001$ nm. The Curie temperature is 430 ± 3 °C. Homogeneous and crackfree samples of about $7\times7\times5$ mm^3 were used to study the lattice vibration spectra using Raman and infrared reflectivity spectroscopy. Compared with the lattice vibration spectra of other TB type crystals, we see that the influence of the Li ions in the *C* sites in the KLN on the characteristic Raman and infrared reflectivity spectra of the Nb-O octahedral ions is striking. Specially, the symmetric bend vibration mode ν_5 was split into three Raman lines, and the antisymmetric stretch vibration mode ν_3 and the antisymmetric bend vibration mode ν_4 were all broadened greatly. [S0163-1829(97)08521-4]

I. INTRODUCTION

During recent years, many related studies[1–5] have suggested that the tetragonal tungsten bronze (TB) type potassium lithium niobate (KLN) single crystal is a potentially useful material for nonlinear optical applications because it is remarkably stable to intense laser radiation and has excellent second harmonic generation (SHG) and secondary electro-optic effects. Specially, it is expected to be a useful material for the blue laser radiation by SHG in a wavelength range from 790 to 920 nm, which takes place at room temperature and enables noncritical phase matching.[2] Also, it has found applications in the surface acoustic wave and piezoelectric devices. However, some of its undesirable properties have limited its practical applications. A big problem is that the KLN crystals are easy to crack when cooling through the paraelectric-ferroelectric phase transition. The useful bulk of centimeter dimensions was not obtained due to cracks induced by the change of composition and structural characteristics. Also, the change of composition in KLN crystal affects the electro-optical and nonlinear optical effects because of the considerable change of the birefringence with variation of lithium content.[6] Recently, various fiber KLN crystals grown by the laser-heated pedestal growth method[4] and the very thin acicular KLN crystals grown by the micro-pulling-down method[5] can provide some practical applications. This paper studies the crystal growth and its lattice vibrational spectra by Raman and infrared reflectivity spectroscopy at room temperature, and compares these spectra with those of other filled and unfilled TB type crystals.

II. EXPERIMENT

The KLN crystals were grown using a pulling method with a Crystalox MCGS-3 system. The starting materials include 99.99% K_2CO_3, Li_2CO_3, and Nb_2O_5. According to the mol fraction of Nb_2O_5 in the phase diagram of KLN crystals,[1] these materials were well mixed. After ballmilling in pure alcohol for 4 h, the mixtures were dried and pressed into disks, with a diameter of 30 mm and a thickness of 25 mm. The disks were put into a 350 ml Pt crucible and melted at 1000 °C by induction heating in air for 12 h. The melt was cooled down to the temperature close to its melting point, and the crystal was pulled from the melt using an SBN:60 seed. The pulling rate was $1-3$ mm/day, and the rotating rate about 30 rpm.

The crystals as-grown along the [100] orientation are cubes about $10\times20\times40$ mm^3, but those grown along the [001] orientation are cylindrical, with a diameter of about 25 mm and a height of 30 mm. In the latter, there is a transparent zone of about $10\times10\times10$ mm^3, with the pale yellow. They were annealed at 800 °C for 24 h to reduce residual stress formed during growth. The crystal structure was checked by a D/MaX-rA x-ray powder diffractometer at room temperature. Their lattice constants calculated are $a=1.2575\pm0.0001$ and $c=0.3997\pm0.0001$ nm. The crystal compositions were determined using a 180–80 atomic spectrum absorptiometer. The molecular formula can be written as $K_{2.96}Li_{1.97}Nb_{5.07}O_{15}$. The Curie temperature is 430 ± 3 °C.

The crystals were cut carefully, along *a*, *b*, and *c* axes, into samples the size of about $7\times7\times5$ mm^3, then were optically polished. These samples are crackfree, homogeneous, and transparent. Room-temperature Raman spectra were measured on a J-Y U-1000 Raman spectrometer with a incident slit width of 100 μm, using a 100-mW argon ion laser at 514.5 nm. Infrared reflectivity spectra at room temperature were obtained by a NIC-20SX FT-IR spectrophotometer with a fitting of Specular Refl. Model 500, using the method

TABLE I. The reducible representations for $P4bm$ at Γ point.

Seitz operator		{1[000] |0}	{2[001] |0}	{4$^+$[001] |0}	{4$^-$[001] |0}	{m[010] |T(1/2, 1/2,0)}	{m[100] |T(1/2, 1/2,0)}	{m[110] |T(1/2, 1/2,0)}	{m[1$\bar{1}$0] \|T(1/2, 1/2,0)}
Position	$8d$	24	0	0	0	0	0	0	0
and	$4c$	12	0	0	0	0	0	2	2
character	$2b$	6	−2	0	0	0	0	2	2
	$2a$	6	−2	2	2	0	0	0	0

of difference spectrum,[7] the controllable resolution was selected as 1 cm^{-1}, and the infrared reflection radiation was collected 60 times.

III. GROUP THEORETICAL CONSIDERATIONS FOR LATTICE VIBRATIONS

The KLN single crystal has a completely filled TB type structure with the filling formula $(A1)_2(A2)_4(C)_4(B1)_2(B2)_8O_{30}$ and the space group $P4bm$ at room temperature. There are the two chemical formulas of the KLN in a unit cell. The reducible representations for the space group $P4bm$ at the center Γ point of the first Brillouin zone are given in Table I, using The International Table for Crystallography.[8]

Based on the factor group theory, the reducible representations shown in Table I can be reduced as follows:

$$8d: 3A_1+3A_2+3B_1+3B_2+6E;$$

$$4c: 2A_1+1A_2+1B_1+2B_2+3E;$$

$$2b: 1A_1+1B_2+2E;$$

$$2a: 1A_1+1A_2+2E.$$

The atomic positions in the KLN crystal are shown in Table II with the aid of the experimental results in Ref. 9.

Using the results shown in Table II, the irreducible representations of the lattice vibration of the KLN crystal are the following:

$$21A_1+16A_2+15B_1+20B_2+39E.$$

Also, the Raman- and infrared-active optic phonon modes are obtained, in terms of the character table of the point group 4mm, as follows:

$$\Gamma_{\text{vib}}=20A_1(R,\text{IR})+15B_1(R)+20B_2(R)+38E(R,\text{IR}).$$

where R and IR represent Raman and infrared active, respectively. It is clear that theoretically observable Raman peaks and infrared reflection bands are not more than 131 and 58 in number, respectively. The Raman scattering tensors are[10]

$$A_1(Z):\begin{bmatrix} a & 0 & 0 \\ 0 & a & 0 \\ 0 & 0 & b \end{bmatrix},\quad B_1:\begin{bmatrix} c & 0 & 0 \\ 0 & -c & 0 \\ 0 & 0 & 0 \end{bmatrix},\quad B_2:\begin{bmatrix} 0 & d & 0 \\ d & 0 & 0 \\ 0 & 0 & 0 \end{bmatrix},\quad E(X):\begin{bmatrix} 0 & 0 & e \\ 0 & 0 & 0 \\ e & 0 & 0 \end{bmatrix},\quad E(Y):\begin{bmatrix} 0 & 0 & 0 \\ 0 & 0 & e \\ 0 & e & 0 \end{bmatrix}.$$

The symmetry species $A_1(Z)$, $E(X)$, and $E(Y)$ show dipole moments oriented along the Z, X, and Y directions, respectively. Due to equivalence of the axes X and Y for the measurement of Raman spectra of uniaxial crystals with the point group $4mm$,[11] the interesting scattering configurations are $X(ZZ)Y$, $X(YZ)Y$, $X(YX)Y$, and $X(YY)Z$, corresponding to the symmetry species A_1, E, B_2 and (A_1+B_1), respectively. Obviously, for the scattering geometry $X(YY)Z$, the symmetry and the vibrational mode of the extraordinary optical phonons are undefined because of an angle of 45° included between the phonon wave vector and the optical axis, which can roughly show the directional dispersion of the extraordinary phonons. For the measurements of the infrared reflectivity spectra, the electric fields of the incident light are aligned along the Z direction for the symmetry species A_1 with the longitudinal dipole moments and perpendicular to the Z direction for the symmetry species E with the transverse dipole moments, respectively. We have seen that the lattice vibration spectra of the octahedral ion $[NbO_6]^{7-}$ in some crystals, such as the unfilled TB type SBN crystal with the point group $4mm$,[12] the filled TB type BNN crystal with the point group $2mm$,[13] and the non-TB type $LiNbO_3$

TABLE II. The atomic position.

Atom	Position	Lattice site
Nb(1)	$2b$	$B1$
Nb(2)	$8d$	$B2$
0.873 K(1)/0.127 Li	$2a$	$A1$
0.989 K(2)/0.011 Li	$4c$	$A2$
0.942 Li/0.058 Nb	$4c$	C
O(1)	$8d$	
O(2)	$8d$	
O(3)	$4c$	
O(4)	$2b$	
O(5)	$8d$	

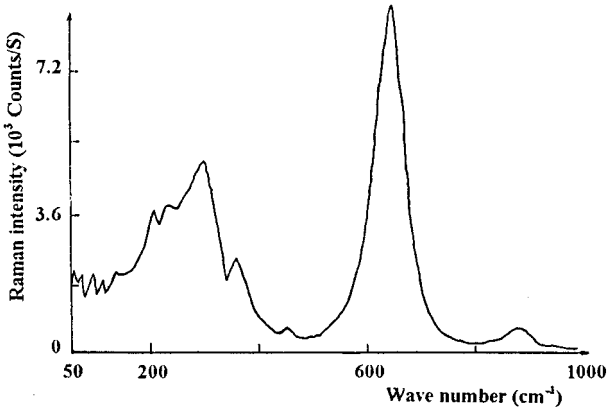

FIG. 1. Raman spectrum recorded in the KLN at 298 K for the symmetry species A_1 with the scattering geometry $X(ZZ)Y$, which concerns extraordinary transverse optical phonons propagating along the [110] direction.

crystal,[14] are similar to each other and show a common characteristic. An octahedral molecule XY_6 with the symmetry O_h has 15 internal vibrational degrees of freedom or six

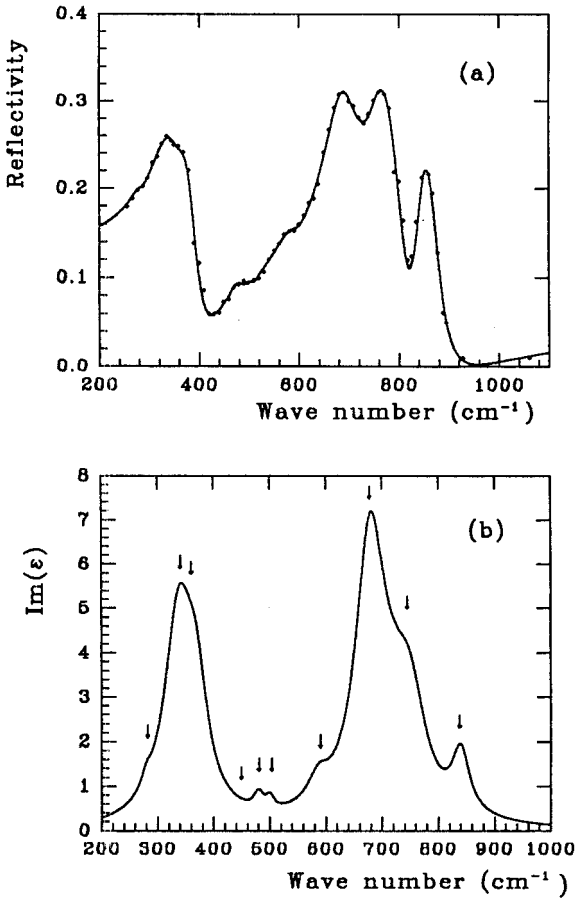

FIG. 2. (a) Infrared reflectivity spectrum recorded in the KLN at 298 K with the electric field of the incident light along the c direction for the symmetry species A_1. The data are shown by the points and the theoretical fit by the solid curve. (b) The dispersion curve of the imaginary part of the permittivity. The arrows point out the resonance frequencies of the oscillators.

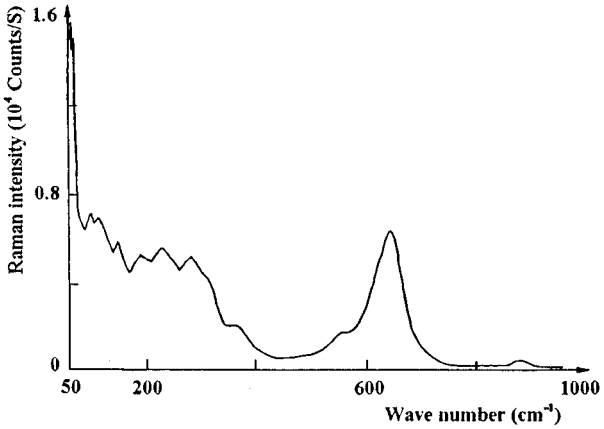

FIG. 3. Raman spectrum recorded in the KLN at 298 K for the symmetry species E with the $X(YZ)Y$ configuration, involving ordinary transverse and extraordinary longitudinal optical phonons propagating along the [110] direction.

normal vibrational modes ν_i. They can be represented from group theoretical considerations as

$$\Gamma'_{\text{vib}} = A_{1g}(R) + E_g(R) + 2T_{1u}(\text{IR}) + T_{2g}(R) + T_{2u}(\text{inactive}),$$

where the subscripts g and u represent symmetric and antisymmetric vibrations, respectively. ν_1, ν_2, and ν_3 are all stretch vibration modes and ν_4, ν_5, and ν_6 are all bend vibration modes. Thus there might be three characteristic Raman peaks and two strong characteristic infrared reflection bands belonging to the internal vibrational modes of the octahedral ion $[NbO_6]^{7-}$ in the KLN crystal. In a primitive cell of the KLN crystal, there are ten Nb-O octahedral ions. Hence, in the experiments, the observable Raman peaks and infrared reflection bands are much fewer in number than those calculated by the group theory.

IV. RESULTS

Figure 1 shows a typical Raman spectrum of the crystal with the octahedral ions, recorded in the KLN at room tem-

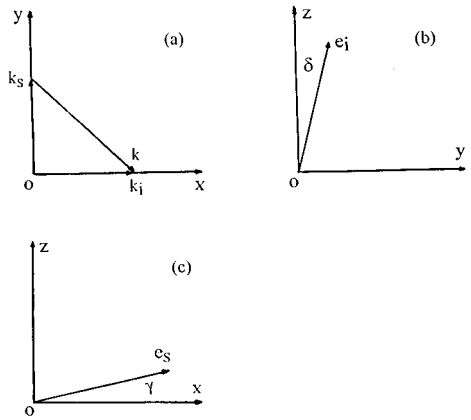

FIG. 4. A selected scattering geometry (a), the polarization direction e_i of the incident light (b), and the polarization direction e_s of the scattering light (c). γ is an angle parameter and δ is an angle variable.

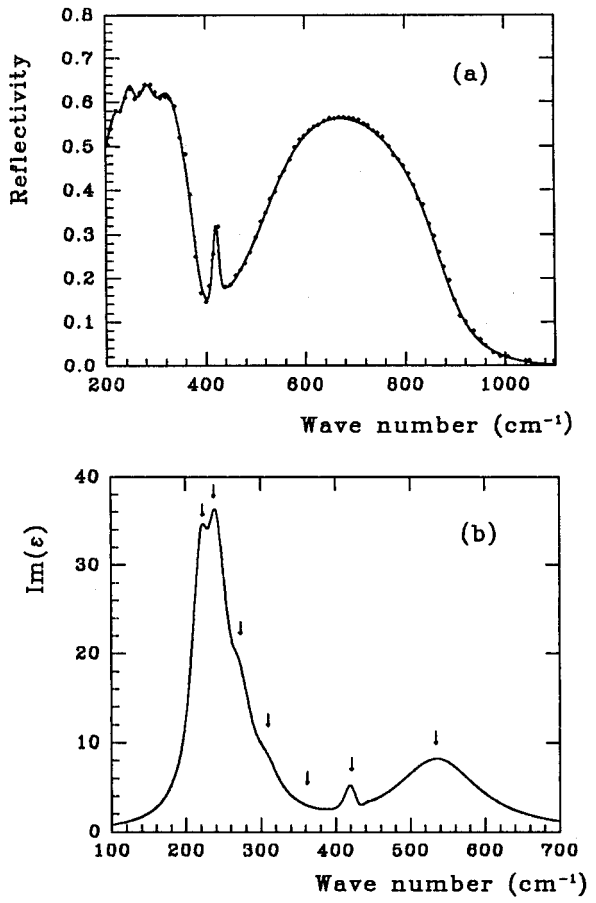

FIG. 5. (a) Infrared reflectivity of the KLN for the ordinary ray. The data are shown by the points and the theoretical fit by the solid curve. (b) The dispersion curve of the imaginary part of the permittivity. The arrows point out the resonance frequencies of the oscillators.

perature in a frequency range from 50 to 1000 cm^{-1}, with the scattering geometry $X(ZZ)Y$, corresponding to the symmetry species A_1 and concerning extraordinary transverse optical phonons propagating along the [110] direction. Compared with the Raman spectrum of the SBN,[12] it is easy to determine two of the three characteristic Raman peaks of $[NbO_6]^{7-}$ in the KLN to be 876(ν_1) and 645(ν_2) cm^{-1}, the third (ν_5) might be split into 207/238/290 cm^{-1} for every $B1$ site and $B2$ site in the KLN possess a distorted octahedron and deviation from O_h symmetry will result in line broadening or even splitting. The modes ν_1 and ν_2 were only broadened but not split, the splitting of the mode ν_5 might be the result of the influence of the Li ions in the C sites on the internal vibrations of $[NbO_6]^{7-}$. The occurrence of a peak of 352 cm^{-1} which belongs to an external vibrational mode for $[NbO_6]^{7-}$ is attributable to the Li ions which caused a polar lattice vibration.

Figure 2(a) is a typical infrared reflectivity spectrum for the crystal with the octahedral ions, recorded in the KLN at room temperature in a frequency range from 200 to 1100 cm^{-1}, corresponding to the A_1 symmetry representation with dipole moments oriented along the c direction. Compared with the same spectrum recorded in the KNSBN,[15] the resonance (transverse) frequencies of the two

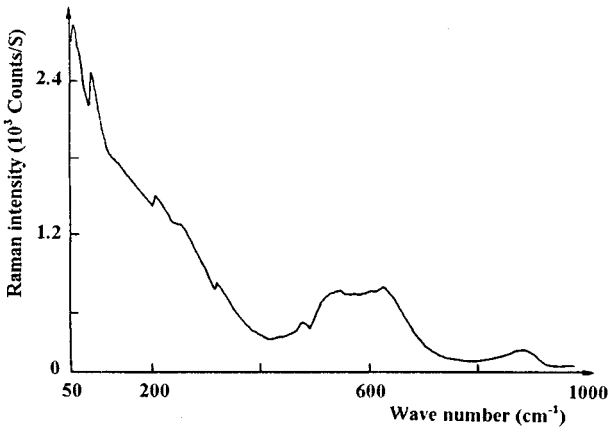

FIG. 6. Raman spectrum of nonpolar lattice vibration modes recorded in the KLN at 298 K, belonging to the symmetry species B_2 with the $X(YX)Y$ scattering configuration.

characteristic infrared-active optical phonon modes of $[NbO_6]^{7-}$ in the KLN are assigned by a classical multioscillator fit[16] to be 680(ν_3) and 340(ν_4) cm^{-1} as shown in Fig. 2(b). We notice the great broadening of the modes ν_3 and ν_4. There are three weak reflection bands, originated from the external vibration for $[NbO_6]^{7-}$, superposed on the strong stretch vibration band, and their resonance frequencies fitted are 587, 742, and 840 cm^{-1}, respectively. On the strong bend vibration band, there are five superposed weak reflection bands with the fitted resonance frequencies of 280, 352, 447, 480, and 500 cm^{-1}, respectively. We can see that, from Fig. 2(a), the influence of the weak bands on the strong bands is very striking when the weak bands are superposed around the longitudinal frequency of the strong bands. No reflection band in the frequency range from 1100 to 4800 cm^{-1} is observed. And from 50 to 200 cm^{-1}, the reflection bands of the external vibration are very weak and not plotted for the ratio of signal/noise degrades.

Figure 3 shows a room-temperature Raman spectrum of the KLN for the $X(YZ)Y$ scattering configuration, which corresponding to the symmetry species E and involves ordi-

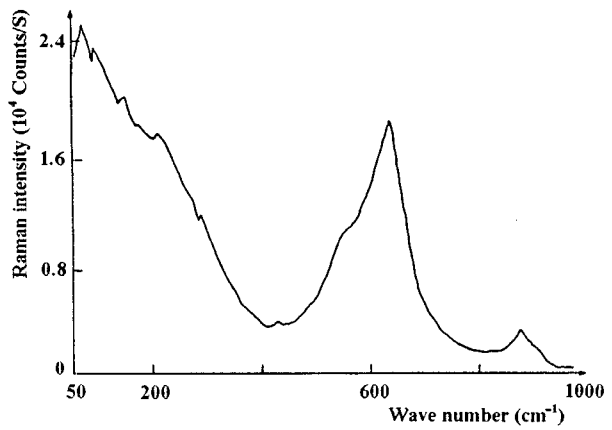

FIG. 7. Raman spectrum recorded in the KLN at 298 K, with the scattering geometry $X(YY)Z$ with an angle of 45° included between the phonon wave vector and the optical axis.

TABLE III. The assignments of the lattice vibration for the KLN (values in cm^{-1} except $\Delta\epsilon$).

Symmetry species	$A_1(Z)$	$E(XY)$	B_2	$A_1(E)+B_1$
Raman	α_{ZZ}	α_{YZ}	α_{YX}	α_{YY}
results	(TO)	54/59 (TO/LO)	58	54
	58	91 (TO+LO)	91	74
	77	116 (TO+LO)	215	91
	91	145 (TO+LO)	273	153
	108	182 (TO+LO)	327	180
	133	223/269/297 (TO+LO,ν_5)	513	207
	207/238/290(ν_5)	360 (TO+LO)	542	290
	352	550 (TO+LO)	632	426
	447	641 (TO+LO,ν_2)	897	542
	480	876 (TO+LO,ν_1)		632
	500			876
	645(ν_2)			
	876(ν_1)			

Infrared	ω_{TO}	ω_{LO}	$\Delta\epsilon$	Γ_d	ω_{TO}	ω_{LO}	$\Delta\epsilon$	Γ_d
results	280	285	0.020	20.0	220	222	0.407	30.0
	340(ν_4)	345(ν_4)	0.900	65.0	238(ν_4)	245(ν_4)	0.902	30.0
	352	367	0.250	45.0	272	274	0.107	40.0
	447	449	0.003	12.0	307	310	0.092	45.0
	480	482	0.015	20.0	360	362	0.012	65.0
	500	503	0.009	17.0	420	426	0.014	10.0
	587	592	0.045	45.0	540(ν_3)	550(ν_3)	0.809	135.0
	680(ν_3)	688(ν_3)	0.600	65.0				
	742	744	0.200	65.0				
	840	846	0.060	37.0				
		$\epsilon_0=2.1984\pm0.0002$				$\epsilon_0=2.0412\pm0.0002$		
		$\epsilon=4.2970\pm0.0002$				$\epsilon=4.3842\pm0.0002$		
		$\Sigma\Delta\epsilon=2.102$				$\Sigma\Delta\epsilon=2.343$		

nary transverse and extraordinary longitudinal optical phonons propagating along the [110] direction. In Fig. 3, only one pair of transverse/longitudinal (TO/LO) modes, split owing to the polar lattice vibrations, was recorded as 54/59 cm^{-1}. Obviously, the action of long-range static force in the lattice of the KLN is not striking, and this crystal polar lattice vibration is slightly stronger than that in the SBN. Compared with Fig. 1, the count intensity of the low-wave-number peaks increases largely.

Here, separating TO and LO modes is simply discussed as follows. (1) A scattering geometry is selected as shown in Fig. 4 and has a relation given as

$$X[(Z+\Delta Y)(X+\Delta Z)]Y=X(ZX)Y+X(\Delta YX)Y+X(Z\Delta Z)Y+X(\Delta Y\Delta Z)Y.$$

In Fig. 4, if the angle $\delta\rightarrow0$ and the angle $\gamma\rightarrow0$, then $X[(Z+\Delta Y)(X+\Delta Z)]Y\rightarrow X(ZX)Y$. (2) In the view of Loudon,[10] the scattering effectiveness is calculated as

$$S_1|_{\delta\rightarrow0,\gamma\rightarrow0}=S_1(E^o_{TO})=0.5e^2\alpha^2\cos^2(\delta-\gamma),$$

$$S_2|_{\delta\rightarrow0,\gamma\rightarrow0}=S_2(E^e_{TO})=0.5e^2(\alpha+\beta)^2\cos^2(\delta+\gamma),$$

where e is a scattering tensor element, α is a constant, β is directly proportional to polarization field strength, γ is an angle parameter, δ is an angle variable, and the superscripts o and e of the mode E represent the ordinary and extraordinary optical phonons, respectively. Therefore,

if $\delta=\gamma$, then S_1 has a maximum $(S_1)_{max}$ and $\delta_1>0$,

if $\delta=-\gamma$, then S_2 has a maximum $(S_2)_{max}$ and $\delta_2<0$,

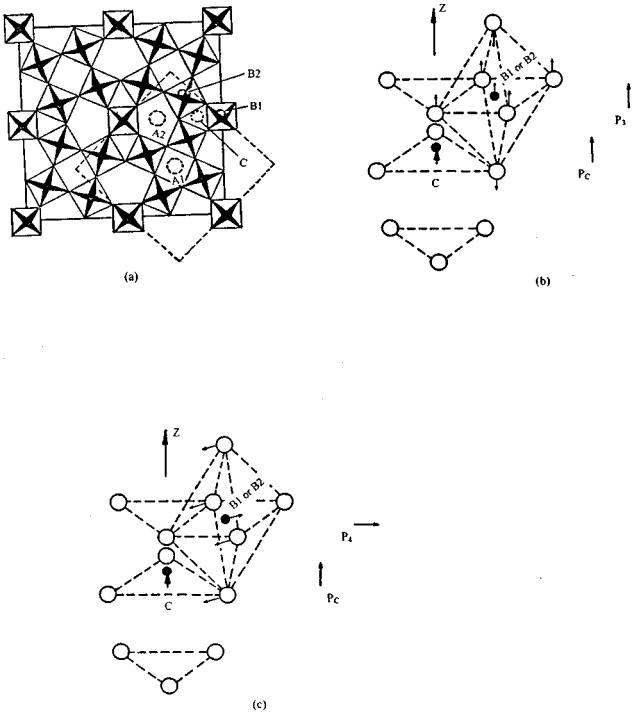

FIG. 8. (a) Schematic diagram of TB type structure projection along [001]. The orthorhombic cell and the tetragonal cell are shown by solid line and dotted line, respectively. (b) Schematic diagram of instantaneous orientations of the dipole moments P_c and P_3. (c) Same as (b) for P_c and P_4.

i.e., δ_1 and δ_2 are strictly symmetric on the longitudinal axis (S axis). (3) For a degenerate mode, wave number $\nu(\mathrm{TO}) = \nu(\mathrm{LO})$, then

$$S_3|_{\delta\to 0,\gamma\to 0} = S_3(E) = S_1(E^o_{\mathrm{TO}}) + S_2(E^e_{\mathrm{LO}})$$
$$= 0.5e^2\alpha^2\cos^2(\delta-\gamma)$$
$$+ 0.5e^2(\alpha+\beta)^2\cos^2(\delta+\gamma).$$

When δ is selected as some value δ_3 between δ_1 and δ_2, the maximum $(S_3)_{\max}$ emerges. As seen, it is easy to judge and to calculate the degenerate modes or the TO/LO splitting modes by selecting the angle γ and changing the angle δ in the experiments.

Recorded in the KLN at room temperature, the infrared reflectivity spectrum of the symmetry species E with the transverse dipole moments is shown in Fig. 5(a). The resonance frequencies of the modes ν_3 and ν_4 are fitted as 540 and 238 cm^{-1} as shown in Fig. 5(b). There is a great influence of a weak band, with a fitted resonance frequency of 420 cm^{-1}, on the bend vibration band. Also, no reflection band is observed above 1100 cm^{-1}, and between 50 and 200 cm^{-1}, the measurements are similar to those mentioned above.

Nonpolar lattice vibration modes, belonging to the symmetry species B_2, are observed in the KLN at room temperature with the $X(YX)Y$ scattering configuration, and the Raman spectrum is shown in Fig. 6. In a unit cell, the atoms of the KLN are five more in number than those of the SBN, but the Raman lines in Fig. 6 are not more than those of the SBN measured under the same conditions. It roughly implies that short-range molecular force in the KLN is weaker than that in the SBN, and this weakened anisotropism would affect the piezoelectric properties of the KLN crystal. It is well known that the piezoelectric constants d_{33} of the KLN and the SBN:60 are 52×10^{-12} and 130×10^{-12} C/N, respectively.[1]

Figure 7 shows a room-temperature Raman spectrum of the KLN, with the scattering geometry $X(YY)Z$ with the angle of 45° included between the phonon wave vector and the optical axis. For the Raman spectra measured in the SBN, only the Raman spectra of the $X(YY)Z$ and the $Y(XX)Z$ were measured to be not equivalent, which was explained as the randomness of vacancy of the A sites, but in the KLN there is no such phenomenon. Comparing Fig. 7 with Figs. 1 and 3, there are E modes in Fig. 7, which roughly implies that the directional dispersion of the extraordinary phonons in the KLN is striking.

In fact, for the TB type crystals, whether their TB type structure is filled or unfilled, all Raman lines except the three characteristic Raman lines, originating from the external vibration for $[\mathrm{NbO_6}]^{7-}$ and showing mainly at the low wave number, are very broad. The count background of all scattering configurations at the low wave number is very strong. It shows the influence of the distorted octahedral ions $[\mathrm{NbO_6}]^{7-}$ on the external vibrations.

The frequency assignments of the lattice-vibration modes of the KLN crystal and the relative parameters are reported in Table III, where α_{zz}, etc. represent the polarizability tensor elements, $\Delta\epsilon$ is the oscillator strength, Γ_d is the damping constant, ϵ_0 is the short-wavelength dielectric constant, and ϵ is long-wavelength dielectric constant.

V. DISCUSSION

Comparing Fig. 5(a) with Fig. 2(a), the infrared reflectivity in Fig. 5(a) is larger than that in Fig. 2(a). It implies that the influence of the external electric field of the incident light on the dipole moment depends on its orientation, and the interaction between the longitudinal external electric field and longitudinal dipole moments is weaker than that between the transverse external field and the transverse moments. We know that, in general, the stronger the interactions between dipole moments and electric field, the higher the interaction energy is, and the less stable the dipole moments are. Hence Figs. 2(a) and 5(a) imply that the influence of the external field on the dipole moment oriented along the C axis are the weakest. That is to say, the longitudinal moment is more stable than the transverse moment in the external field. If the KLN crystals are polarized into a single domain, the polarization will be stable for some period of time.

In the KLN crystal the C site is nine coordinated (Fig. 8).[9] The influence of the Li ions in the C sites on the modes ν_3 and ν_4 is shown in Figs. 8(b) and 8(c), respectively, where the P_c represents an additional dipole moment caused by the Li ion's absolute atomic displacement of 0.0114 nm from the mean oxygen atom layer involving an O(4) and two O(5). The P_3 represents the longitudinal dipole moment originating from the antisymmetric stretch vibration of $[\mathrm{NbO_6}]^{7-}$ with the mode ν_3; and the P_4 represents the transverse dipole moment originating from the antisymmetric bend vibration of $[\mathrm{NbO_6}]^{7-}$ with the mode ν_4. It is rather difficult to

exactly explain the influence of the P_c on the P_3 and the P_4. However, in terms of the dipole-dipole interactions, Figs. 8(b) and 8(c) intuitively show that the dipole moment P_3 is more stable than the dipole moment P_4, when the dipole moment P_c occurs.

As mentioned above an Li ion in the *C* site is slightly displaced from the plane formed by the three nearest oxygen ions. The average Li-O distance to these nearest oxygen neighbors is 0.2153 nm.[9] The six next-nearest oxygen-ion neighbors form a trigonal prism about the Li ion at an average Li-O distance of 0.2542 nm. The short Li-O distance is very close to the average Li-O distances measured for six coordinated Li, e.g., 0.2176 nm in $LiTaO_3$,[17] 0.2153 nm in $LiNbO_3$,[18] and 0.2148 nm in Li_2TiO_3.[19] It can be seen that the influence of the Li ion in the *C* site on the internal vibrations of $[NbO_6]^{7-}$ is very strong so as to largely broaden the modes ν_3 and ν_4 and completely split the mode ν_5. However, why the Li ions in the *C* sites have almost no influence on the symmetric stretch vibration modes ν_1 and ν_2 and are similar to those measured in other filled and unfilled TB type crystals is still unknown. Also, why some infrared-active modes, e.g., 587, 742, 840 cm^{-1}, etc., are not recorded in Raman spectra is difficult to explain, too.

VI. CONCLUSIONS

The experimental results reported show that the Nb-O octahedral ion $[NbO_6]^{7-}$ in its entirety in the KLN is apparent based on three reasons. (1) The measured vibrational modes are much fewer in number than those calculated by group theory because of the larger $[NbO_6]^{7-}$ in the unit cell. (2) The larger damping constants are selected to fit the curves because of the larger damping force originated from the nonharmonic interaction of the ions including $[NbO_6]^{7-}$ with the larger ion mass. (3) The modes $\nu_1-\nu_5$ can approximately represent the internal vibration characteristic of $[NbO_6]^{7-}$ with O_h symmetry.

Comparing the lattice-vibration spectra of the KLN with those of other TB type crystals, such as the SBN and the KNSBN crystals, we can see that the influence of the Li ions in the *C* sites on the characteristic Raman and infrared-reflectivity spectra of $[NbO_6]^{7-}$ in the KLN is striking. As mentioned above, the change of lithium content in the KLN affects the electro-optical and nonlinear optical effects. Possibly, because the *C* sites are completely occupied by the Li ions the KLN is easy to crack. Understanding what the origin of crack might be, how to overcome this problem, and intensifying the crystal electro-optical effect and nonlinear optical effect are obviously subjects of significance. Perhaps, a new KLN crystal with incompletely filled TB-type structure is worth study.

ACKNOWLEDGMENTS

This work was supported by the Natural Science Foundation and State Key Laboratory of Crystal Materials of Shandong University of China.

*Present address: Experimental Centre, Shandong University, Jinan 250100, P. R. China.

†Present address: Department of Computer Science, Shandong University, Jinan 250100, P. R. China.

[1] R. R. Neurgaonkar, W. K. Cory, J. R. Oliver, and L. E. Cross, Mater. Res. Bull. **24**, 1025 (1989).

[2] J. J. E. Reid, Appl. Phys. Lett. **62**, 19 (1993).

[3] D. H. Yoon, M. Hashimoto, and T. Fukuda, Jpn. J. Appl. Phys. **33**, 3510 (1994).

[4] J. K. Yamamoto, S. A. Markgraf, and A. S. Bhalla, J. Cryst. Growth **123**, 423 (1992).

[5] D. H. Yoon, P. Rudolph, and T. Fukuda, J. Cryst. Growth **144**, 207 (1994).

[6] L. G. Van Uitert, H. J. Levinstein, J. J. Rubin, C. D. Capio, E. F. Dearborn, and W. A. Bonner, Mater. Res. Bull. **3**, 47 (1968).

[7] J. L. Koenig, Appl. Spectrosc. **29**, 295 (1975).

[8] *International Tables for Crystallography, Vol. A: Space-Group Symmetry*, edited by T. Haha (Reidel, Dordrecht, 1983).

[9] S. C. Abrahams, P. B. Jamieson, and J. L. Bernstein, J. Chem. Phys. **54**, 2355 (1971).

[10] R. Loudon, Adv. Phys. **13**, 423 (1964); Errata: **14**, 621 (1965).

[11] S. M. Liu and G. Y. Zhang, Acta Phys. Sin. **32**, 657 (1983).

[12] H. R. Xia, K. X. Wang, B. Y. Zhao, H. C. Chen, X. L. Lu, Q. Z. Jiang, P. J. Sun, and L. J. Hu, Acta Phys. Sin. **45**, 232 (1996).

[13] A. Boudou and J. Sapriel, Phys. Rev. B **21**, 61 (1980).

[14] R. F. Schaufele and M. J. Weber, Phys. Rev. **152**, 705 (1966).

[15] H. R. Xia, H. C. Chen, H. Yu, L. J. Hu, K. X. Wang, and B. Y. Zhao, Phys. Rev. B **54**, 8954 (1996).

[16] W. G. Spitzer and D. A. Kleinman, Phys. Rev. **121**, 1324 (1961).

[17] S. C. Abrahams, W. C. Hamilton, and A. Sequiera, J. Phys. Chem. Solids **28**, 1693 (1967).

[18] S. C. Abrahams, J. M. Reddy, and J. L. Bernstein, J. Phys. Chem. Solids **27**, 997 (1966).

[19] J. F. Dorrian and R. E. Newnham, Mater. Res. Bull. **4**, 179 (1969).